Evaluation of Heat Treatments for Additively Manufactured 316L

J. Simpson*, L. Donovan*, R. Dehoff*, T.S. Byun*, C. Joslin*

*Oak Ridge National Laboratory, 1 Bethel Valley Road, PO Box 2008, Oak Ridge, TN 37831

Simpsonjj@ornl.gov

ABSTRACT

316L stainless steel is frequently chosen for load bearing applications in nuclear power plants due to its good creep resistance, radiation damage resistance, and a large existing database and characterization for nuclear application. The rapid meltpool solidification of laser powder bed fusion results in high internal stresses that in turn necessitate stress relief heat treatments at a minimum. In this work, a factorial design of experiments to evaluate the effects of different lasers, quenching vs furnace cooling, and stress relief vs solution heat treatment vs HIP was conducted to quantify the effect of various heat treatments on microstructures and mechanical property outcomes.

INTRODUCTION

Additive manufacturing (AM) is one of the transformative technologies that is being demonstrated as rapid and cost effective solution for deployment of advanced nuclear reactors under the Transformational Challenge Reactor (TCR) program [1]. AM poses unique challenges and opportunities for materials characterization and process control due to the high number of process variables and common occurrence of detrimental features such as pores. Conversely, the metallic AM components fabricated by laser powder bed fusion (L-PBF) may offer superior properties with respect to irradiation void swelling resistance because the rapid solidification rate of the meltpool limits grain size growth under certain conditions [2].

L-PBF fabricates components by sequentially melting thin (20 - 100µm) layers of metal feedstock powder into the geometry of the desired component with a focused laser. The small meltpool and rapid solidification result in fine grain size distributions and high residual stresses, which must be relieved. Hot isostatic pressing (HIP) is a frequently utilized post-process in nuclear reactor applications to reduce porosity; however, the temperatures required for HIP (~1100°C) effectively solution heat treats 316L and may result in detrimental grain growth. The effects of heat treatments on additively manufactured 316L have previously been reported for fatigue [3], hardness and wear resistance [4], [5], and tensile properties [5], [6]. However, to the authors' knowledge no studies to date have been published for 1) evaluating inter-laser heat treated tensile property variation, or 2) comprehensively comparing stress relief, solution and HIP treatments.

EXPERIMENTAL METHODS

316L was additively fabricated into 13mm diameter 65mm long cylinders oriented in the Z axis in a single build with a Concept Laser M2 and ASTM E8 tensile test specimens were machined from the cylinders; the same laser parameter of 370W power, 1350mm/s velocity, 130µm spot size, 90µm hatch spacing, 10mm stripe width, 67° inter-layer rotation, and 50µm layer thickness with the snaking strategy illustrated in Figure 1 was used to fabricate all specimens. A single lot of recycled argon gas atomized 316L powder from Praxair (TruForm 316-3) with a vendor measured D10=18µm, D50=31 µm, D90=49 µm size distribution and chemical composition of Table 1 was used for fabrication; SEM observation of the feedstock powder revealed generally spherical powder with some satellites as seen in Figure 2.
An overview image of the build is provided in Figure 3 for reference. Group 1 per the experimental layout in Table 2 was treated and rapidly quenched within a HIP

Figure 1: Snaking Laser Scan Strategy Used in Fabrication

Table 1: Feedstock Chemical Composition

Element	ASTM F3184-16 (wt %)	Measured (wt %)
C	<0.030	0.006
Co	-	0.10
Cr	16.0 – 18.0	17.07
Cu	-	0.01
Fe	Bal	Bal
Mn	<2.00	1.19
Mo	2.00 – 3.00	2.41
N	-	0.01
Ni	10.00 – 14.00	12.08
O	-	0.05
P	<0.045	<0.005
S	<0.030	0.004
Si	<1.00	0.46

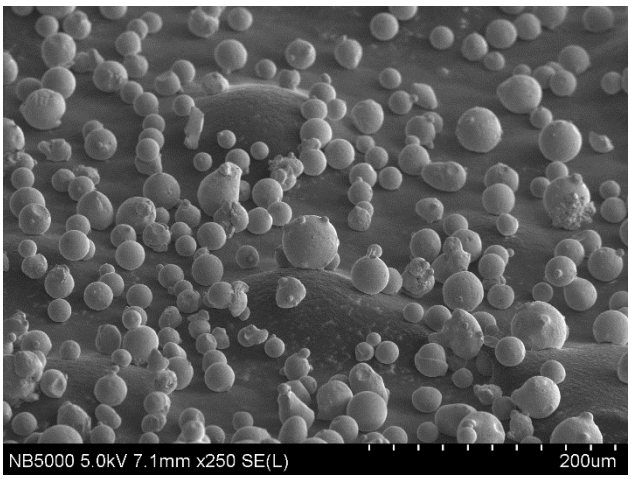

Figure 2: SEM Image of 316L Feedstock

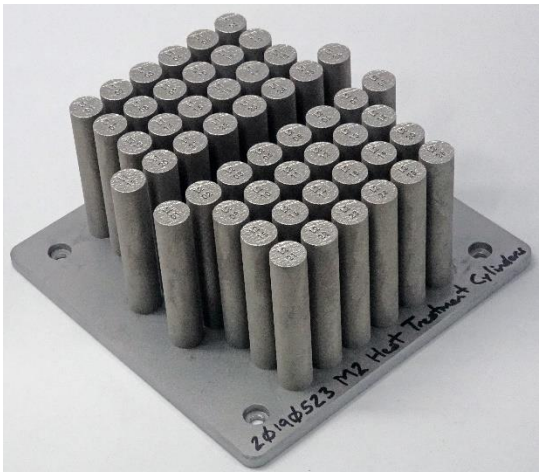

Figure 3: Build Overview

Table 2: Experimental Design

Temperature	1100°C	1100°C	650°C
Time	60 mins	60 mins	30 mins
Pressure	100MPa	0 MPa	0 MPa
Quench	**Group 1**	**Group 2**	**Group 4**
Furnace Cool (10°C/min)	-	**Group 3**	**Group 5**

furnace (Quintus Technologies model QIH), and all other quenched groups were quenched by placing on a large steel heat sink and air cooling. Samples for all groups other than group 1 were sealed in quartz tubes with partial pressure argon (0.25 atm) and heat treated in the same furnace (CM Furnaces model 1730-20HT). A factorial combination for furnace cooled HIP samples was not possible due to machine restrictions. All samples were heated at 10°C/min and utilized high purity argon (99.999%).

Four replicates per heat treatment factorial combination were fabricated on each of the AM machine's two lasers and tensile tested per ASTM E8; select mounted sub-samples from each group were analyzed via optical microscopy, scanning electron microscopy (SEM), electron backscatter diffraction (EBSD), and scanning transmission electron microscopy (STEM). Etching was conducted with 10g oxalic acid dissolved in 100ml distilled water by electrolytically etching at 50-60mA for 6 minutes.

RESULTS

One tensile test specimen (Laser 1 – Group 1) was damaged during loading and is not included in results. Mean tensile test results and standard deviations are tabulated in Table 3; 2D optical porosity measurements at were obtained for a single specimen from each group – laser combination. A 4 way MANOVA test with Yield Strength (YS), Ultimate Tensile Strength (UTS), Uniform Elongation, and Total Elongation as dependent variables and Lasers, Temperature, Pressure, and Cooling Methods as independent variables was conducted using the R package "stats v3.6.2" from the CRAN repository as follows:

```
> model = lm(cbind(`YS (MPa)`,`UTS (MPa)`, `Uniform Elongation (%)`, `Total Elongation (%)`) ~ (`Treatment Temperature (°C)`+`Pressure (MPa)`+Cooling+Laser), data = Heat)

> summary(manova(model))
```

MANOVA results are presented in Table 4; Temperature, Pressure, and Lasers were found to be significant at the 0.05 confidence level while differing

Table 3: Mean and Standard Deviation Tensile Results and 2D Porosity

Group		YS (MPa)	UTS (MPa)	Uniform Elongation (%)	Total Elongation (%)	2D Optical Porosity (%)
Total Population		344.89 (33.47)	600.25 (16.24)	56.18 (3.43)	72.34 (4.00)	0.012-0.158
Laser 1	Sub-Population	345.14 (35.01)	598.31 (11.16)	56.54 (3.67)	72.67 (4.19)	0.022-0.158
	Group 1	310.42 (2.48)	587.58 (2.43)	60.08 (0.52)	75.76 (2.00)	0.022
	Group 2	323.68 (15.54)	600.16 (29.94)	59.62 (1.17)	75.19 (3.46)	0.135
	Group 3	319.58 (2.23)	590.53 (1.99)	59.05 (0.53)	75.44 (1.60)	0.158
	Group 4	382.77 (2.11)	610.60 (1.84)	52.48 (0.60)	69.95 (3.94)	0.142
	Group 5	383.70 (5.31)	610.82 (2.30)	52.37 (0.37)	67.77 (1.53)	0.117
Laser 2	Sub-Population	344.65 (32.85)	602.10 (20.06)	55.83 (3.24)	72.03 (3.90)	0.012-0.149
	Group 1	310.42 (2.48)	587.58 (2.43)	59.89 (1.16)	76.49 (3.61)	0.012
	Group 2	323.68 (15.54)	600.16 (29.94)	56.96 (2.11)	70.36 (3.40)	0.119
	Group 3	319.58 (2.23)	590.53 (1.99)	57.60 (0.64)	74.33 (2.81)	0.149
	Group 4	382.77 (2.11)	610.60 (1.84)	52.35 (0.21)	69.95 (2.34)	0.139
	Group 5	383.70 (5.31)	610.82 (2.30)	52.36 (0.28)	69.01 (1.69)	0.126

Table 4: MANOVA Results - Statistical Significance of Main Variables

	Df	Pillai	approx F	num Df	den Df	Pr(>F)	
`Treatment Temperature (°C)`	1	0.99246	1020.22	4	31	< 2.2e-16	***
`Pressure (MPa)`	1	0.56937	10.25	4	31	2.094e-05	***
Cooling	1	0.05884	0.48	4	31	0.7470	
Laser	1	0.31354	3.54	4	31	0.0172	*
Residuals	34						

Signif. codes: 0 ‘***’ 0.001 ‘**’ 0.01 ‘*’ 0.05 ‘.’ 0.1 ‘ ’ 1

Cooling Methods were not found to have a statistically significant effect. Scatterplots with distribution kernel density estimations (KDE) in the margins are provided in Figure 4 for graphical representation of the tensile data.

Optical un-etched images of mounted specimens contained predominantly spherical pores characteristic of keyholing [7]–[9]. Etched optical images taken in the XZ plane revealed negligible microstructural variation between as-fabricated and stress relieved specimens. HIPed specimens no longer contained meltpool outlines in etched optical images but distinct directional orientations were observed. A composite image of etched and polished optical images for representative as-fabricated, stress relieved, and HIP samples is provided in Figure 5. The solution heat treated microstructure was indistinguishable from the HIP microstructure and therefore not included. Nano-scale Si rich oxide inclusions were observed in all mounted specimens; a representative STEM image of inclusions is presented in Figure 6.

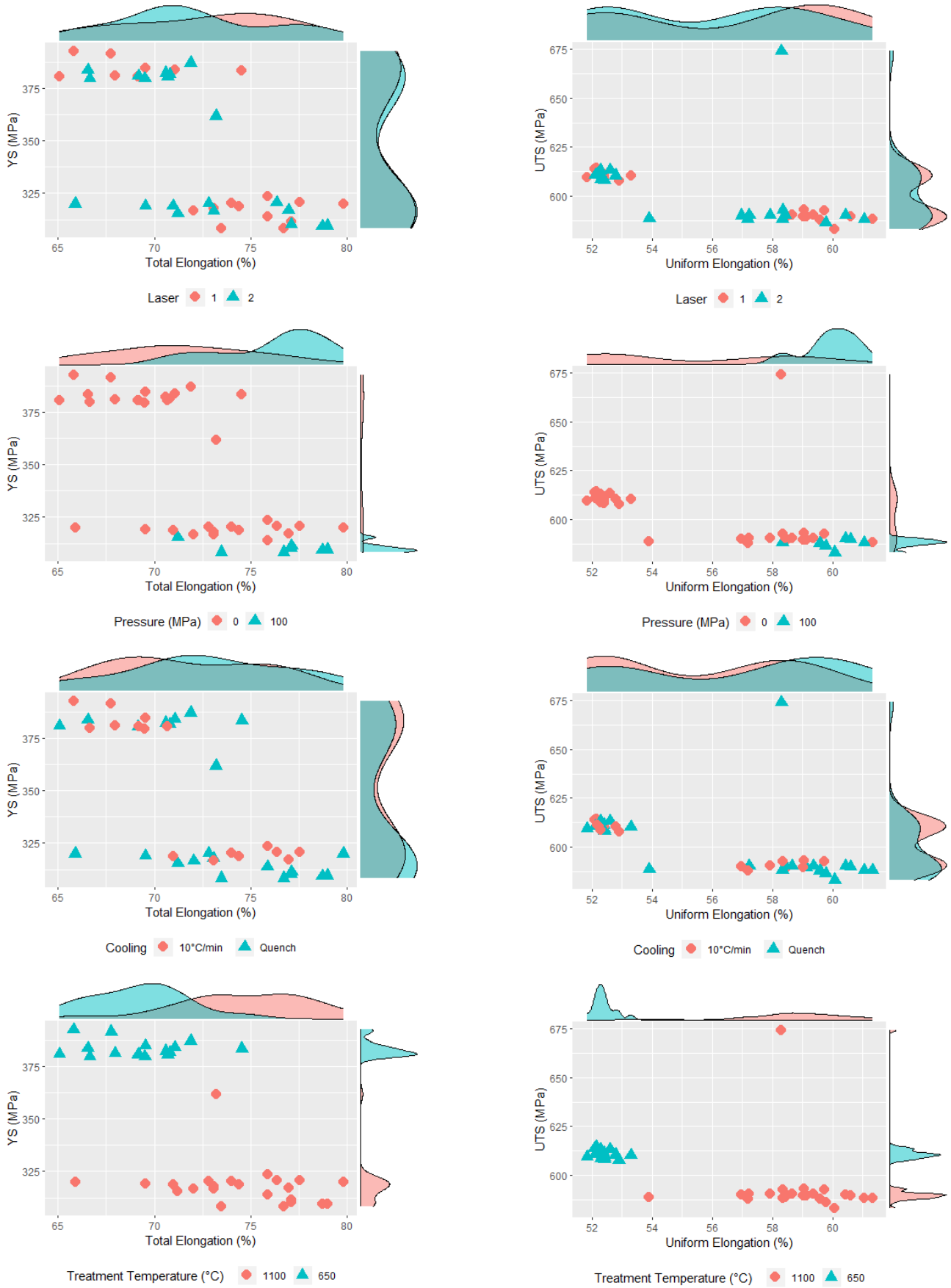

Figure 4: Graphical Representation of Tensile Data. Left Column) Total Elongation (%) vs Yield Strength (MPa) Right Column) Uniform Elongation (%) vs Ultimate Tensile Strength (MPa) Row 1) Segmented by Laser Row 2) Segmented by Treatment Pressure (MPa) Row 3) Segmented by Cooling Method Row 4) Segmented by Treatment Temperature (°C)

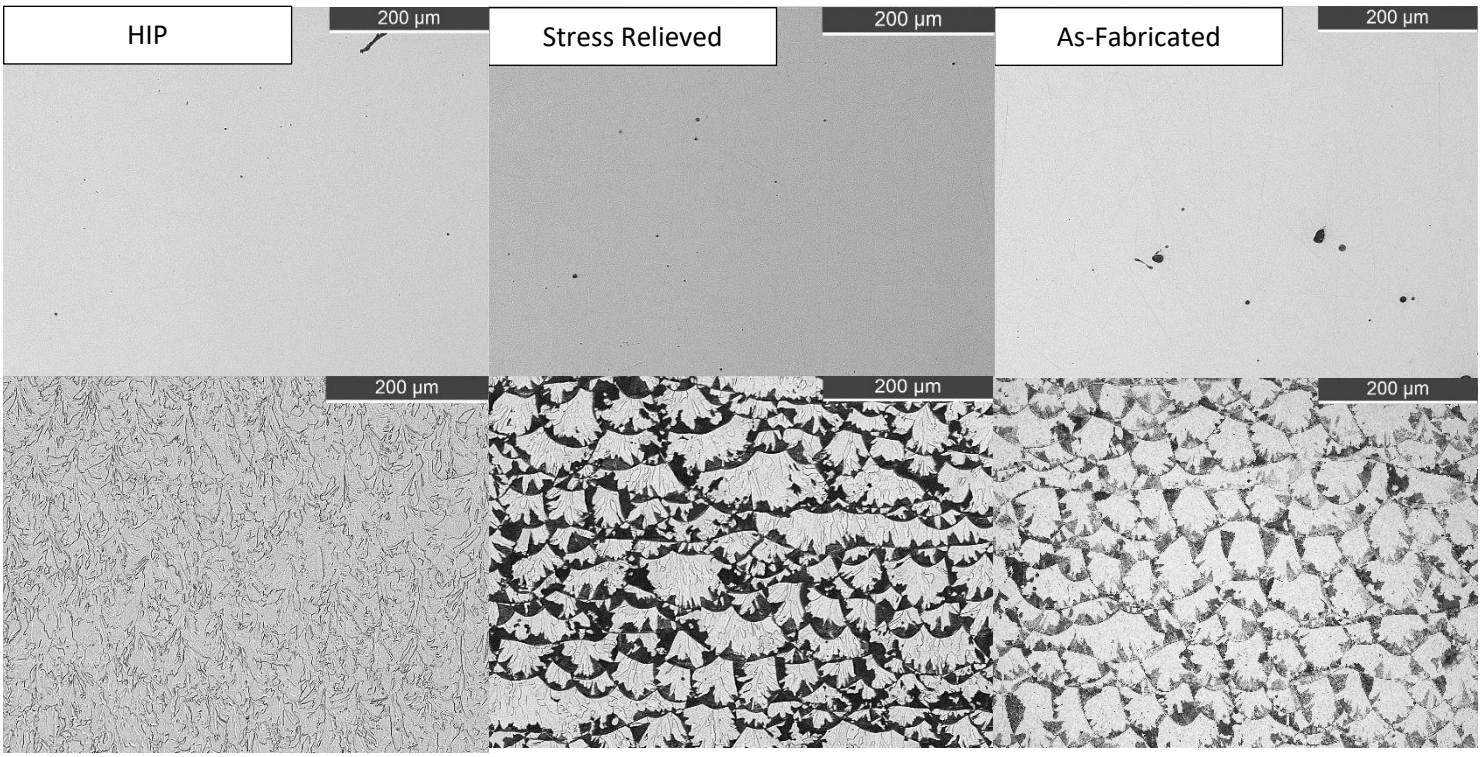

Figure 5: 316L Microstructures, 1st Row) Un-etched Optical, 2nd Row) Etched Optical

DISCUSSION

In general, heat treatment temperature is the primary explanatory variable of tensile properties as it results in grain growth. YS and UTS decreases due to grain growth are predicted by the Hall Petch relationship and the increase in ductility due to grain growth is predicted by the ease of intra-grain dislocation movement versus grain boundary sliding. A statistically significant though perhaps not functionally meaningful effect is observed due to HIPing pressure which slightly decreases strength and increases ductility. Multiple ANOVA analyses were run post-MANOVA and detected a statistically significant difference in uniform elongation due to different lasers at the 0.05 confidence level, suggesting that either laser calibration variation or as-of-yet unquantified intra-machine variation may be in effect. All factorial combinations resulted in tensile properties exceeding ASTM F3184-16 requirements of YS >30KSI, UTS >75KSI and elongation >30%, suggesting that additively manufactured 316L heat treatment selection for nuclear power plant applications should not be constrained by tensile property considerations. Work by Rebak et. al. [10] has indicated that stress corrosion cracking (SCC) in stress relieved L-PBF 316L pulled parallel to the build direction and HIPed L-PBF 316L is comparable to wrought conventional 316L, but stress relieved L-PBF 316L pulled perpendicularly to the build direction had a crack growth rate approximately three times greater than conventional wrought 316L. Mechanistically, SCC cracks in stress relieved samples grew through columnar grains when pulled in the build direction and intra-granularly when pulled perpendicularly to the build direction [10]; similar behavior in crack growth due to orientation has been reported for fatigue crack growth in stress relieved L-PBF 316L [11]. Si and Mn rich nano-scale oxide inclusions at grain boundaries were observed to accelerate the SCC crack growth rate [10], and the interaction of oxide inclusions and intra-granular crack growth mode may explain the accelerated crack growth rates observed for stress relieved L-PBF 316L pulled perpendicularly to the build direction. Si and Mn rich oxide inclusions were observed in this study and have been reported in L-PBF 316L elsewhere [12] and are likely formed by species preferential oxygen scavenging during the fabrication process and / or are present in feedstock. Reducing Si and Mn content, adding more oxygen reactive elements that form SCC resistant oxides, or further reducing oxygen content during fabrication may be possible methods of reducing the occurrence of Si and Mn rich inclusions. Unpublished work by Argonne National Laboratory under the Transformational Challenge Reactor program has

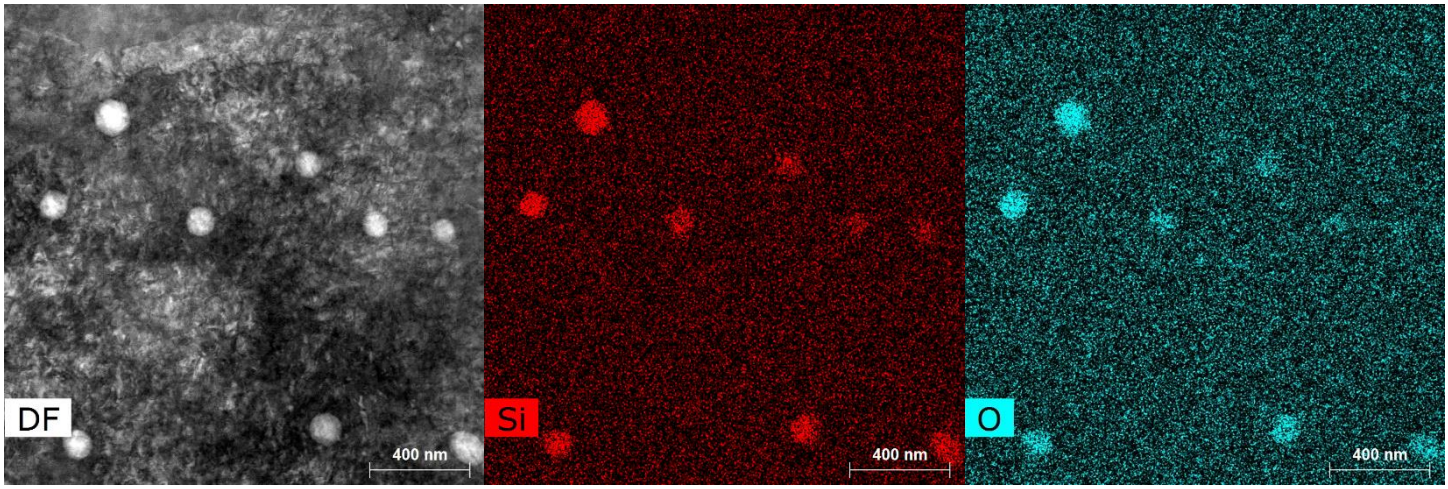

Figure 6: Representative STEM Image of Observed Oxide Inclusions

indicated that stress relief heat treatments offer superior creep resistance relative to as-fabricated and solution heat treated L-PBF 316L, which may be an important consideration depending on component application.

HIP post-process treatments for L-PBF 316L have previously been recommended due to improved irradiation assisted stress corrosion cracking (IASCC) resistance [13] relative to stress relief treatments. High (0.3%) porosity has been reported to accelerate SCC crack growth rates relative to low (0.08%) porosity by approximately 40% [10] all else equal, thereby partially explaining the improved IASCC resistance of HIP post processing. The high temperatures required for HIP also result in grain growth, thereby reducing the grain boundary surface area and the number of oxide inclusions at grain boundaries. However, optimization of L-PBF processing parameters may allow for extremely low (<0.05%) porosity in as-fabricated material, and elimination or reduction of oxide inclusions may be possible via feedstock compositional changes. If those two technical challenges are achieved, HIP may offer no significant benefits relative to solution heat treatments. HIP does not close surface connected pores or cracks [14], therefore the degree of porosity reduction in thin walled components will likely be less than in thick components. Elimination of HIP post processing is desirable as it is a more costly process relative to stress relief and solution heat treatments.

Further work is needed prior to determining an optimal heat treatment for L-PBF 316L for nuclear power plant applications. Specifically, the effects of extremely low as-fabricated porosity and Si-oxide-inclusion free microstructures on sensitive material properties such as fatigue, SCC, and IASCC should be evaluated in addition to conducting replicate studies.

CONCLUSIONS

Laser powder bed fusion 316L was evaluated for the effects of different lasers, heat treatment cooling rate, temperature, and pressure. The following conclusions were drawn from experimental data:

1) Stress relief, solution and HIP heat treatments all result in tensile properties exceeding ASTM F3184-16 requirements, indicating heat treatment selection for L-PBF 316L for nuclear power plant applications should not be constrained by tensile property considerations.
2) Heat treatment temperature, and pressure have statistically significant effects on material tensile properties.
3) Statistically significant differences in post-treatment tensile properties may occur due to different lasers.

ACKNOWLEDGEMENTS

This research was supported by the Transformational Challenge Reactor program supported by the US Department of Energy, Office of Nuclear Energy.

REFERENCES

[1] "Transformational Challenge Reactor," *Oak Ridge National Laboratory*. https://tcr.ornl.gov/.

[2] Z. Shang *et al.*, "Response of solidification cellular structures in additively manufactured 316 stainless steel to heavy ion irradiation: an in situ study," *Mater. Res. Lett.*, vol. 7, no. 7, pp. 290–297, 2019, doi: 10.1080/21663831.2019.1604442.

[3] B. Blinn, F. Krebs, M. Ley, R. Teutsch, and T. Beck, “Determination of the influence of a stress-relief heat treatment and additively manufactured surface on the fatigue behavior of selectively laser melted AISI 316L by using efficient short-time procedures,” *Int. J. Fatigue*, vol. 131, no. April 2019, p. 105301, 2020, doi: 10.1016/j.ijfatigue.2019.105301.

[4] E. Tascioglu, Y. Karabulut, and Y. Kaynak, “Influence of heat treatment temperature on the microstructural , mechanical , and wear behavior of 316L stainless steel fabricated by laser powder bed additive manufacturing,” 2020.

[5] E. Liverani and A. H. A. Lutey, “The effects of hot isostatic pressing (HIP) and solubilization heat treatment on the density , mechanical properties , and microstructure of austenitic stainless steel parts produced by selective laser melting (SLM),” 2020.

[6] T. Ronneberg, C. M. Davies, and P. A. Hooper, “Revealing relationships between porosity, microstructure and mechanical properties of laser powder bed fusion 316L stainless steel through heat treatment,” *Mater. Des.*, vol. 189, p. 108481, 2020, doi: 10.1016/j.matdes.2020.108481.

[7] Z. Francis, “The Effects of Laser and Electron Beam Spot Size in Additive Manufacturing Processes,” *Ph.D. Diss.*, no. May, 2017, [Online]. Available: https://search.proquest.com/docview/1906683857?fromunauthdoc=true&pq-origsite=gscholar%0Ahttp://repository.cmu.edu/dissertations/909.

[8] A. M. Philo *et al.*, “A pragmatic continuum level model for the prediction of the onset of keyholing in laser powder bed fusion,” *Int. J. Adv. Manuf. Technol.*, vol. 101, no. 1–4, pp. 697–714, 2019, doi: 10.1007/s00170-018-2770-7.

[9] L. Scime and J. Beuth, “Using machine learning to identify in-situ melt pool signatures indicative of flaw formation in a laser powder bed fusion additive manufacturing process,” *Addit. Manuf.*, vol. 25, no. October 2018, pp. 151–165, 2019, doi: 10.1016/j.addma.2018.11.010.

[10] R. B. Rebak *et al.*, “Environmental Cracking and Irradiation Resistant Stainless Steels by Additive Manufacturing,” 2018.

[11] A. Riemer, S. Leuders, M. Thöne, H. A. Richard, T. Tröster, and T. Niendorf, “On the fatigue crack growth behavior in 316L stainless steel manufactured by selective laser melting,” *Eng. Fract. Mech.*, vol. 120, pp. 15–25, 2014, doi: 10.1016/j.engfracmech.2014.03.008.

[12] X. Sun, F. Chen, H. Huang, J. Lin, and X. Tang, “Effects of interfaces on the helium bubble formation and radiation hardening of an austenitic stainless steel achieved by additive manufacturing,” *Appl. Surf. Sci.*, vol. 467–468, no. October 2018, pp. 1134–1139, 2019, doi: 10.1016/j.apsusc.2018.10.268.

[13] M. Song, M. Wang, X. Lou, R. B. Rebak, and G. S. Was, “Radiation damage and irradiation-assisted stress corrosion cracking of additively manufactured 316L stainless steels,” *J. Nucl. Mater.*, vol. 513, pp. 33–44, 2019, doi: 10.1016/j.jnucmat.2018.10.044.

[14] L. N. Carter, M. M. Attallah, and R. C. Reed, “Laser powder bed fabrication of nickel-base superalloys: influence of parameters; characterisation, quantification and mitigation of cracking,” in *Superalloys 2012: 12th International Symposium on Superalloys*, 2012, pp. 577--586.